ANALOG VLSI SYSTEM FOR ACTIVE DRAG REDUCTION

Bhusan Gupta

Rodney Goodman

Fukang Jiang

Yu-Chong Tai

California Institute of Technology

Steve Tung

Chih-Ming Ho

University of California, Los Angeles

Drawing inspiration from the structure of shark skin, the authors are building a system to reduce drag along a surface.

In today's cost-conscious air transportation industry, fuel costs are a substantial economic concern. Drag reduction is an important way to increase fuel efficiency and reduce these costs. Even a 5% reduction in drag translates into estimated savings of millions of dollars in annual fuel costs.

Organized structures that play an important role in turbulence transport may cause large skin friction drag. Commonly observed near-wall streamwise vortices cause high drag in turbulent flows (Figure 1, next page). The interaction of these vortices, which appear randomly in both space and time, with the viscous layer near a surface creates regions of high surface shear stress. This stress, when integrated over a surface, contributes to the total drag.

Previous attempts to reduce drag by controlling turbulent flows focused on ways to prevent the formation or limit the strength of these vortices. However, the microscopic size of these vortices, which decreases as the Reynolds number of the flow increases, has limited physical experimentation. Further limiting analytical approaches is the inherent complexity of the nonlinear Navier-Stokes equations.

Can biology tell us something?

In many complex problems, we often find inspiration by observing how nature has evolved biological systems. For drag reduction, deep-sea sharks serve as potential biological models because they are highly evolved predators with a 350-million-year lineage. Deep-sea sharks (for example, hammerheads) swim as fast as 20 meters per second (72 kilometers per hour) in deep water. The exact physiology of these species remains a mystery because they are difficult to study: Replicating the deep-sea setting in a controlled environment is difficult.

Biologists know, however, something about the scales (dermal denticles) that cover the shark's skin. Only recently, researchers[1] found that a denticle has a microscopic structure (Figure 2). The natural argument about evolution would lead one to conclude that the scales' structure assists a shark's movement, perhaps indicating some method of drag reduction.

The entire question of active control of shark skin is speculative. Biologists hypothesize[2] that sharks actively move their denticles. Indirect evidence of this is twofold. The denticles connect to muscles underneath the shark's skin. The total number of mechanoreceptive pressure sensors (pit organs) and their placement on a shark's body positively correlate with the speed of the species. For good active control, the shark may need many sensors to relay the current condition over its body. Although questions remain about sharks using active control, we concluded from this biological example that it may be beneficial to use controlled microscopic structures to reduce drag.

How small is small?

By examining drag patterns in a wind tunnel at velocities between 10 and 20 m/s (36 and 72 km/hr), we narrowed the scope of the problem to extract usable statistics. The drag-inducing vortex pair streaks vary as the Reynolds number of the flow changes. A typical airflow of 15 m/s (54 km/hr) in the wind tunnel achieves a Reynolds number of about 10^4. This, in turn, gives the vortex streaks a statistical mean width of about 1 millimeter. The length of a typical vortex streak can be about 2 centimeters for a 20-to-1 aspect ratio. The average spacing between streaks is about 2.5 millimeters, and the mean rate of appearance of the streaks is approximately 100 Hz. A chaotic process best describes the appearance and disappearance of these vortex pairs.

Numerical simulations demonstrated that suppressing the interaction between streamwise vortices and the wall[3] achieves significant drag reduction (about 25%). These experiments in computational fluid dynam-

0272-1732/96/$5.00 © 1996 IEEE

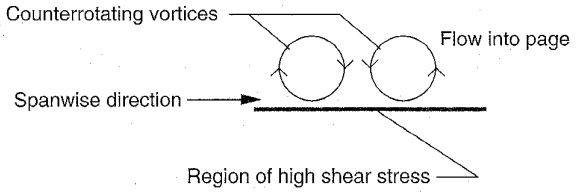

Figure 1. Diagram of the interaction between a vortex pair and the wall showing the high shear stress (hence drag) region created by the pair of counterrotating streamwise vortices.

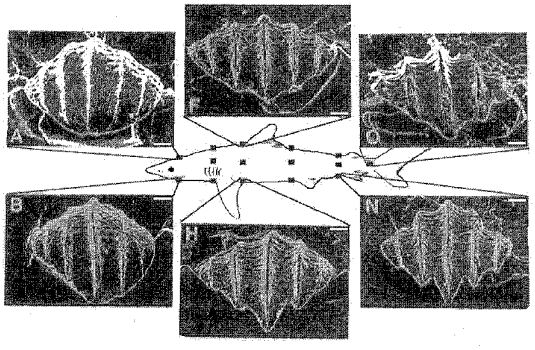

Figure 2. Examples of *Carcharhinus falciformis* shark scales. (White bar = 25 µm.) (Courtesy of *Australian J. Marine and Freshwater Research,* 1992.)

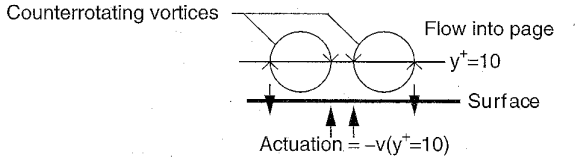

Figure 3. Simple control law that demonstrates the required actuation at the wall boundary achieves a significant drag reduction.

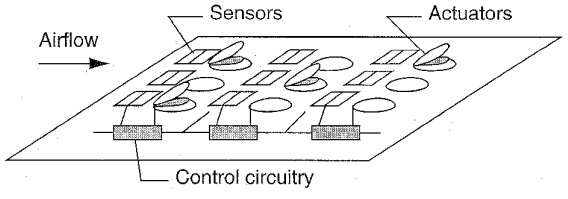

Figure 4. Simplified diagram of the hardware system.

ics incorporated active feedback control to achieve this goal.

Our experimental control scheme involved blowing and suction at the wall according to the normal component of the velocity field. This normal component (at a small distance from the surface in a parallel plane at $y^+ = 10$) is sensed in the near-wall region away from the surface (see Figure 3). Apparently, a simple control law that pushes the areas of high shear stress away from the wall helps minimize the overall drag. This observation formed the basis for the system we wanted to build.

Definitions

Denticles: Conical, pointed projections such as scales on a shark's skin.

Form drag: Motion resulting from the presence of a boundary layer; also known as pressure drag.

Hammerhead sharks: Medium-size shark family that has eyes at the ends of lateral extensions of the flattened head.

Microactuator: Mechanical device built using silicon micromachining; typically less than 1 mm in size.

Micromachining: Technology combining silicon VLSI processing and mechanics to produce mechanical structures at microscopic scale.

MOSIS: Metal-Oxide Semiconductor Implementation Service, a US chip fabrication facility for universities.

Navier-Stokes equations: Equations describing viscous-fluid flow.

Reynolds number: Number characteristic of a fluid's flow past an obstruction.

y^+: Nondimensional unit of distance normalized by the Reynolds number in fluid mechanics.

System details

We wanted to combine the technologies of silicon micromachining and analog VLSI to build an integrated system that actively strives to reduce surface drag. We used micromachining technology to construct fluid sensors and actuators on the same scale as the vortex pairs. To build the dense circuits required to process signals in real time for an integrated system, we used analog VLSI technology.

Our system (Figure 4) incorporates VLSI control circuitry along with microscopic sensors and actuators that can actively deform a surface to reduce drag. Figure 4 shows the physical layout of our system—both sensors and actuators cover the surface controlled by circuitry underneath.

Circuits process the signals from the sensors to find regions of high shear stress. This detection process uses information about the spatial and temporal nature of the streaks. First, the long and narrow aspect ratio leads to building "column"-oriented templates for streak detection. We organized the sensor outputs into thin feature detectors oriented in the direction of the airflow. When several sensors in a column (or channel) register either a larger or smaller output than their neighbors in a spanwise direction, this difference accumulates. If this accumulated difference exceeds a threshold, a vortex pair streak may be present in that column. The appropriate control action raises the associated actuator.

Micromachined components. We used silicon micromachining technology for the microsensors and microactuators.[4-6]

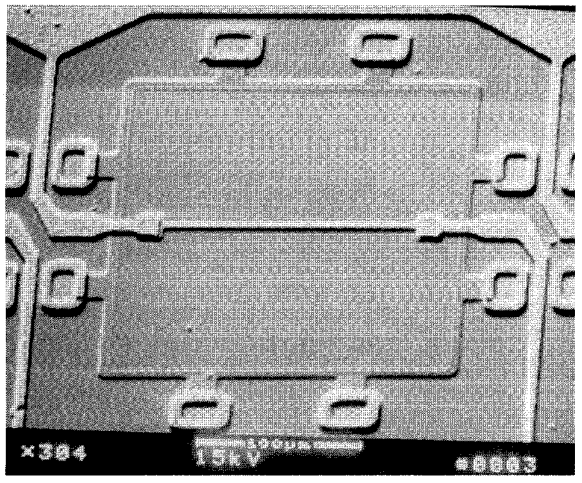

Figure 5. Shear stress sensor showing polysilicon wire over a diaphragm.

Shear stress sensor. The microsensor (Figure 5) measures the heat transfer between a heated wire and the air. Heat transfers by convection from the electrically heated wire to the fluid flow, causing a power change in the polysilicon wire. The polysilicon wire sits on a 200-μm-square, 1.2-μm-thick silicon nitride diaphragm over a vacuum cavity. The 2.0-μm-deep vacuum cavity minimizes thermal losses to the substrate.

A discrete constant temperature circuit (Figure 6) controls the shear stress sensor. This circuit maintains a constant temperature on the heated wire by balancing a bridge. The amplified voltage feedback signal is the output; the overall circuit gain is about 20.

We built the sensors as one row of 25 sensors (Figure 7). This lets us monitor a spanwise section of the wind tunnel. Five sensor outputs (in the middle of the figure) provide inputs to the detection-control chip. Because we have many fewer actuators than sensors, we did not need to use more sensors in the detection experiments.

Microactuator. This device[7] (Figure 8) is a thin plate raised via magnetic actuation. Current moving through a metal coil in the external magnetic field is enough to cause up to a 100-μm deflection. However, the microactuators suffer from the lack of a high mechanical bandwidth. In theory, the resonant frequency of the actuator is about 1 kHz; however, at the present time only a 100-Hz bandwidth can be demonstrated physically.

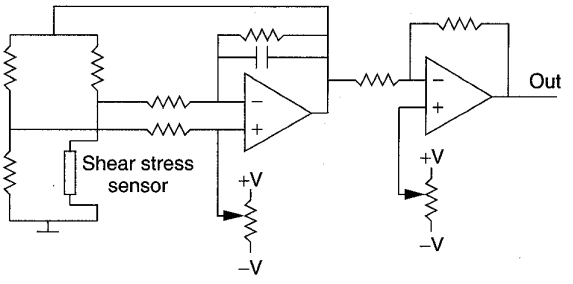

Figure 6. Constant temperature circuit for the shear stress sensor.

Circuits. Figure 9's diagram (next page) shows the information flows in the detection-control chip. A nonlinear filtering network connects the amplified outputs of the shear stress sensors. The filtering preserves large differences between adjacent sensors while smoothing away small differences. The comparison and aggregation operations correspond by columns to different actuators. Once the aggregated signal exceeds a threshold, the system drives the actuator.

Figure 10 depicts a detailed schematic of one column. The output sensor signal of the constant temperature circuit feeds into a further stage of amplification (Figure 11). A buffer (Figure 12) distributes the amplified signal to a nonlinear resistive network composed of H_{RES} circuits[8] (Figure 13).

Sensor outputs in the same column and sensor outputs in adjacent columns use different spatial-filtering constants. The different constants serve to reinforce activity within a col-

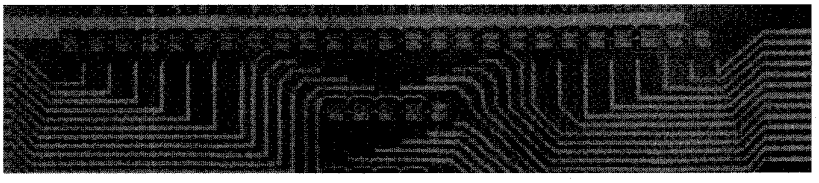

Figure 7. Array of 25 shear stress sensors, which spans a distance of 7.5 mm.

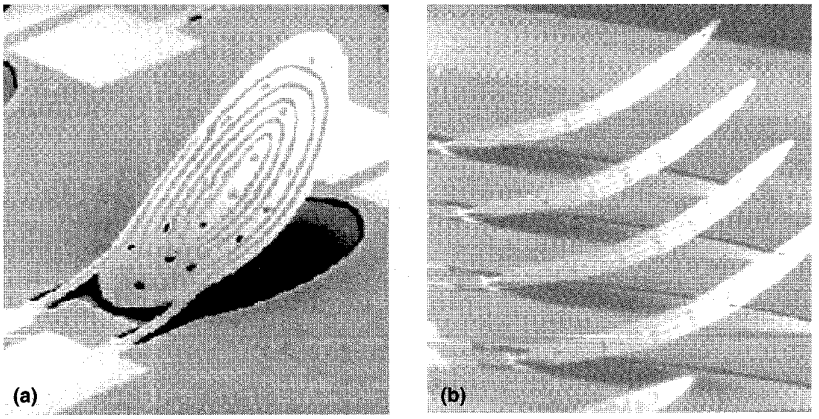

Figure 8. Photograph of a microactuator (a) and an array of microactuators (b).

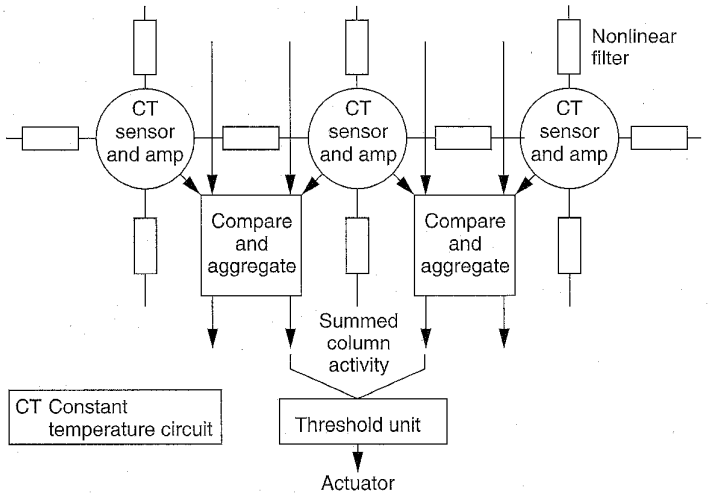

Figure 9. Block diagram of the complete detection-control chip.

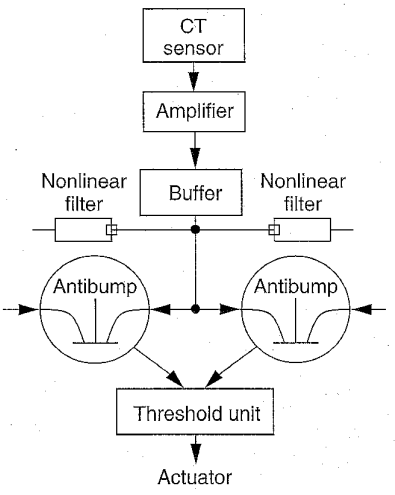

Figure 10. Schematic of one column (channel) of the detection-control circuitry.

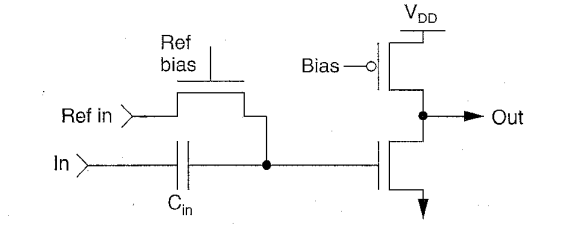

Figure 11. First-stage amplifier.

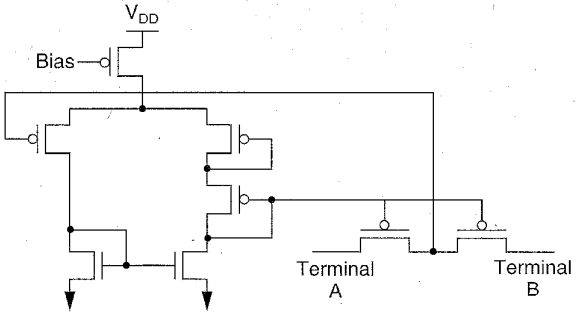

Figure 13. Nonlinear resistor (H_{RES}).

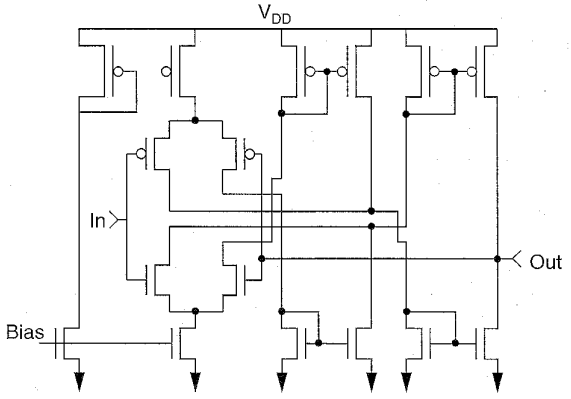

Figure 12. Rail-to-rail buffer amplifier.

umn and discourage activity between adjacent columns.

The filtered signals feed to a symmetric antibump circuit[9] (Figure 14). The circuit's operation mimics a soft comparator with an adjustable dead zone. The circuit indicates when a particular column registers a large shear stress value but the neighboring columns do not. The current output of the antibump circuit accumulates for a particular column, and the circuit shown in Figure 15 compares it to a threshold. If the accumulated value exceeds the threshold, the circuit turns on a pull-down transistor to trigger the actuator.

We used the 2.0-μm CMOS process (that is, Orbit Semiconductor N-well) available through MOSIS to fabricate the detection-control chip shown in Figure 16.

System testing

We used several different experiments to test various system components. First, signal generators presented synthetic signals to the detection-control chip to validate output. Second, mechanical actuators generated known disturbances to verify the response of the system operating in the wind tunnel's laminar regime. Third, the system interacted with a fully turbulent channel flow in the wind tunnel to observe system response.

Results. The overall delay of the processing system is about 40 μs. The amplifier (Figure 11) has a gain-bandwidth product of approximately 500 kHz with the transistors operating in the subthreshold region. The buffer (Figure 12) has a full-power,

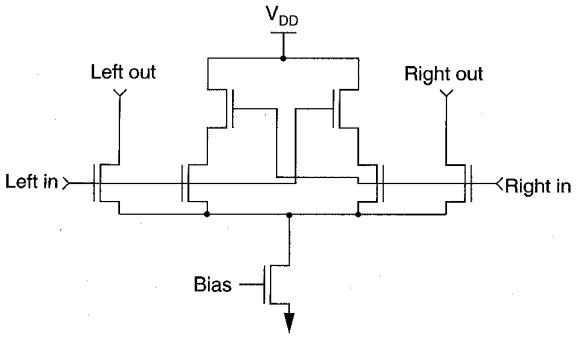

Figure 14. Symmetric antibump circuit.

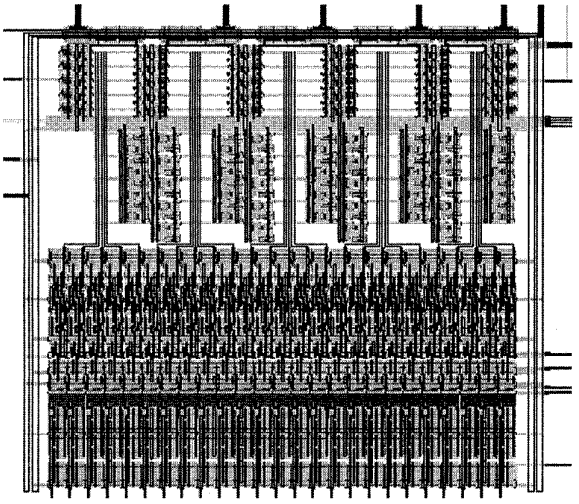

Figure 16. Plot of the detection-control chip.

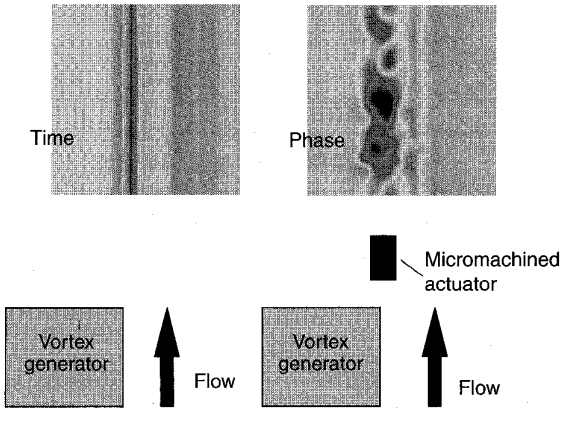

Figure 18. A microactuator's effect on an artificially generated vortex in a laminar flow. The average shear stress on the right-hand plot is approximately 10% less than that on the left-hand, no-actuation plot. Each side shows the exact setup used to generate the image above it.

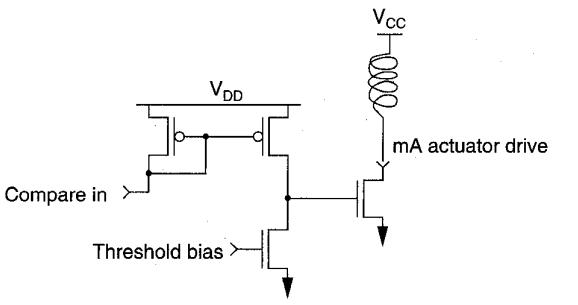

Figure 15. Threshold comparator circuit.

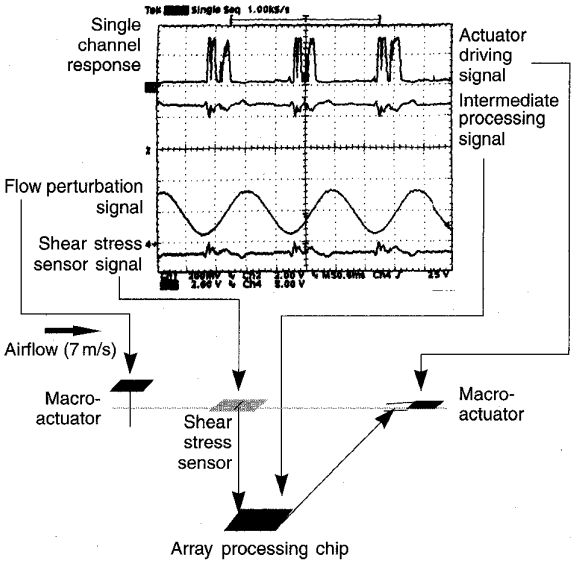

Figure 17. Laminar flow perturbation experiment that demonstrates the ability of the sensor plus electronics to detect disturbances in the laminar flow caused by a periodic actuation.

100-kHz bandwidth. We set the H_{RES} bias to 0.5 V, which corresponds to minimal spreading. We also set the antibump circuit bias for a 160-mV dead zone. The delay of the circuits in Figure 14 and Figure 15 accounts for the remainder of the time delay. The actuator driver can sink about 30 mA at a 1-V drop.

Sample test of system in laminar flow. This experiment consisted of generating a periodic disturbance in a laminar flow to check the response of the signal processing and the actuator movement. We used a macro-size actuator driven by a signal generator to create the disturbance. The perturbation frequency is about 7 Hz, which is reasonable for microactuator response. Figure 17 shows this experiment.

Another experiment ensured that the microactuators can, in fact, reduce drag. We conducted this experiment (depicted in Figure 18) in the laminar-flow regime with an artificially generated vortex pair. Using a periodic driving signal on the actu-

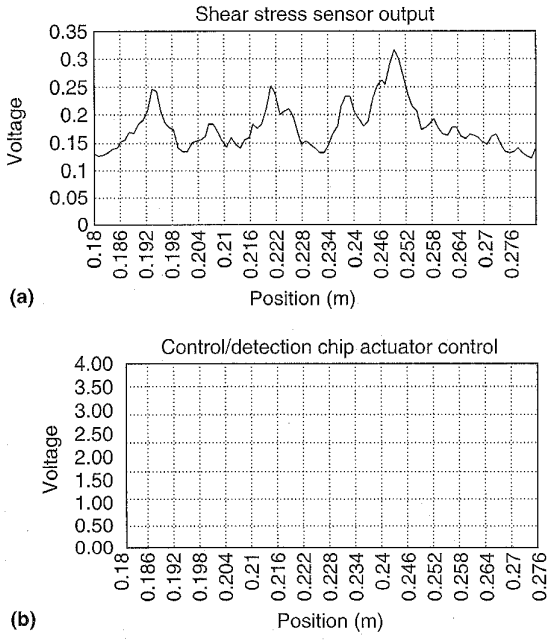

Figure 19. Graph of the output waveforms of one shear stress sensor (a) and the corresponding channel from the detection-control chip (b). We recorded the data in a fully developed turbulent flow.

ators, we measured about a 10% reduction in the average shear stress. This result, however, does not include the consideration of form drag, which would reduce the effectiveness.

Turbulent drag performance. We designed this system to reduce the fully turbulent drag in our experimental setups and presented it with a fully turbulent airflow profile. The centerline velocity of our wind-tunnel channel varies between 10 and 20 m/s (36 and 72 km/hr). Figure 19 graphs the single-column system response.

Figure 20 shows an image of the full field of 25 sensors and the partial five-sensor field used to generate the detection-control output. Figure 21 plots the input-output relationship between wall shear stress and the actuator activation signal. Note that all large shear stress measurements have triggered actuator responses.

In this experiment, the microactuators do not yet have the mechanical frequency response to follow the actuation signals. Thus, we can only roughly estimate the drag reduction that our system provides. We recorded both the outputs of the shear stress sensors and those of the detection-control chip. From our data, we estimated the drag reduction at approximately 2.5%, assuming that the microactuators are about 75% effective in mitigating the high shear stress.

OUR ANALOG VLSI system interfaces with microfabricated, constant-temperature shear stress sensors. It detects regions of high shear stress and outputs a control signal to activate a microactuator. We are in the process of verifying the actual drag reduction by controlling microactuators in wind tunnel experiments. We are encouraged that an approach similar to one that biology employs provides a very useful contribution to the problem of drag reduction.

Our future goal is to demonstrate actual drag reduction with an integrated system. Presently, we are developing technology necessary to place all sensors, actuators, and control circuitry on a single substrate.

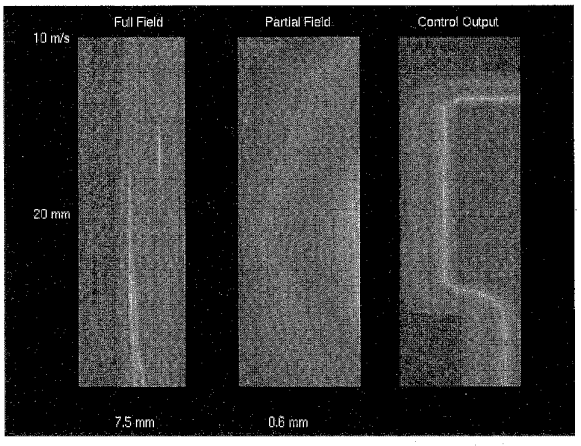

Figure 20. Two-dimensional flow image of instantaneous shear stress. From left to right, we plotted the full span (25-sensor) recording, an enlargement of the middle three sensors, and finally, the output of the detection-control chip corresponding to those three inputs. We recorded the data in a turbulent flow regime with a 10-m/s free-stream velocity and obtained the 2D aspect of the plots by time sampling a 1D span.

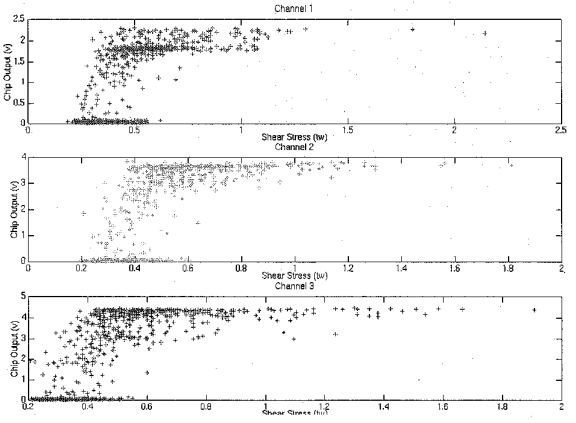

Figure 21. Transfer curve for three channels of the detection-control chip with the data recorded at a 15 m/s flow. The data indicates that for large values of shear stress, the detection-control circuitry would, in fact, turn on an actuator.

Acknowledgments

The Center for Neuromorphic Systems Engineering, as a part of the National Science Foundation Engineering Research Center Program (grant EEC-9402726) and the California Trade and Commerce Agency, Office of Strategic Technology (grant C94-0165) supported this work. Also, ARPA/ONR (grant N00014-93-1-0990) and AFOSR University Research Initiative (grant F49620-93-1-0332) partially supported this work.

References

1. D.W. Bechert, G. Hoppe, and W.-E. Reif, "On the Drag Reduction of the Shark Skin," tech. report 85-0546, Am. Institute of Aeronautics and Astronautics, New York, 1985.
2. W.-E. Reif and A. Dinkelacker, "Hydrodynamics of the Squamation in Fast-Swimming Sharks," *Neues Jahrb. Geol. Paläontol. Abh. [New Yearbook of Geology and Paleontology]*, Vol. 164, 1982, pp. 184-187.
3. P. Moin, J. Kim, and H. Choi, "On Active Control of Wall-Bounded Turbulent Flows," tech. report 89-0960, Am. Institute of Aeronautics and Astronautics, 1989.
4. P.R. Bandyopadhyah, "Development of a Microfabricated Surface for Turbulence Diagnostics and Control," *ASME Application of Microfabrication to Fluid Mechanics,* Am. Soc. of Mechanical Engineers, Chicago, 1994, pp. 67-74.
5. C. Liu et al., "Surface Micromachined Thermal Shear Stress Sensor," *ASME Application of Microfabrication to Fluid Mechanics,* Am. Soc. of Mechanical Engineers, 1994, pp. 9-15.
6. F. Jiang et al., "Polysilicon Structures for Shear Stress Sensors," *Tech. Digest IEEE Tencon 95*, IEEE, Piscataway, N.J.
7. T. Tsao et al., "Micromachined Magnetic Actuator for Active Fluid Control," *ASME Application of Microfabrication to Fluid Mechanics*, Amer. Soc. of Mechanical Engineers, 1994, pp. 31-38.
8. C.A. Mead, *Analog VLSI and Neural Systems,* Addison-Wesley, Reading, Mass., 1989.
9. T. Delbrück, "Bump Circuits for Computing Similarity and Dissimilarity of Analog Voltages," memo 10, Computation and Neural Systems Dept., California Institute of Technology, Pasadena, 1991.

Bhusan Gupta is working toward his PhD in electrical engineering at the California Institute of Technology, Pasadena, California, by studying analog circuits to reduce drag on the microscopic scale. Gupta holds a BS degree in electrical engineering from the University of California, Berkeley, and an MS from Caltech. He is a student member of the IEEE.

Rodney Goodman is a professor of electrical engineering in Caltech's Microsystems Group and director of the multidisciplinary NSF Center for Neuromorphic Systems Engineering. His research areas include intelligent information processing systems and the technologies for endowing next-century machines with the senses of vision, hearing, touch, and smell (chemical sensing).

Goodman holds a BSc from the University of Leeds and a PhD from the University of Kent at Canterbury, both in electrical engineering. He is a member of the IEEE.

Fukang Jiang is working toward his PhD degree at the California Institute of Technology. His research interests include the integration of microsensors, -actuators, and -electronics for active flow control, and the development of advanced packaging technologies such as the flexible-skin-type substrate for MEMS devices.

Jiang received his BS degree in physics from Hangzhou University, People's Republic of China, and his MS degree in electrical engineering from the California Institute of Technology.

Yu-Chong Tai is an associate professor of electrical engineering at the California Institute of Technology. His research interests include developing integrated systems for micromachined solid-state sensors and actuators such as pressure sensors, microphones, and anemometers.

Tai holds a BS from National Taiwan University and MS and PhD degrees from the University of California, Berkeley, all in electrical engineering.

Steve Tung is a postdoctoral researcher in the Fluid Mechanics Laboratory at the University of California, Los Angeles. Previously, he was a lecturer in the Mechanical Engineering Department of the University of Houston. His current research is in active turbulent drag control using MEMS-based microsensors and microactuators.

Tung received his BSME from the National Taiwan University and his PhD from the University of Houston, where his dissertation work examined the development of 3D structures in a shear flow under the influence of acoustic excitation.

Chih-Ming Ho is a professor in the Mechanical and Aerospace Engineering Department and director of the Center for Micro Systems, which he recently established to advance micro-electro-mechanical systems, at the University of California, Los Angeles.

Ho received his PhD in mechanics from the John Hopkins University and his BS degree in mechanical engineering from the National Taiwan University. He was elected a Fellow of the American Physical Society and the American Institute of Aeronautics and Astronautics. He has served as an associate editor of the *ASME Journal of Fluid Engineering* and the *AIAA Journal.*

Direct questions concerning this article to Bhusan Gupta, Department of Electrical Engineering, California Institute of Technology, M/S 136-93, Pasadena, CA 91125; bgupta@caltech.edu.

Reader Interest Survey

Indicate your interest in this article by circling the appropriate number on the Reader Service Card.

Low 168	Medium 169	High 170